This is a repository copy of *High-speed grating interferometry*.

White Rose Research Online URL for this paper:
https://eprints.whiterose.ac.uk/187417/

Version: Published Version

High-speed grating interferometry

Marathe, Shashidhara, Ziesche, Ralf, Das, Gunjan, Schroeder, Sven, Baird, Emily, et al.

SPIE.

High-speed grating interferometry

Shashidhara Marathe,[1, a] Gunjan Das,[1-3] Sven L. M. Schroeder,[1-3] Ralf Ziesche,[1] Emily Baird,[4] and Christoph Rau[1]

[1]*Diamond Light Source Limited, Harwell Science and Innovation Campus, Fermi Ave, Didcot OX11 0DE, UK*
[2]*School of Chemical and Process Engineering, University of Leeds, 211 Clarendon Rd, Leeds LS2 9JT, UK*
[3]*Research Complex at Harwell, Rutherford Appleton Laboratory, Didcot OX11 0FA, UK*
[4]*Stockholm University, Zoologiska institutionen: Funktionell zoomorfologi, 106 91 Stockholm, Sweden*

a) Corresponding author: shashidhara.marathe@diamond.ac.uk

ABSTRACT

We present the most recent advances in fast X-ray grating interferometer and their applications. A dedicated setup for rapid scanning with a single grating and using filtered broadband illumination of an undulator source has been implemented. With this setup, grating interferometer tomographic scans can be achieved within few minutes owing to the filtered broadband beam and single-grating spatial harmonic imaging technique. Use of this system on the chemical processes happening in few millisecond time span is presented. This beam condition is very stable which is very difficult to achieve with the monochromatic beams. Tomographic phase volume rendering obtained with this beam condition is explained. We will also describe the new capabilities and applications.

Keywords: X-ray grating interferometer, Talbot Imaging, phase-contrast imaging, spatial harmonic imaging, tomography, high-speed imaging, pink-beam, high-throughput imaging, anti-solvent crystallization, continuous crystallisation

1. INTRODUCTION

The X-ray Grating Talbot Interferometer (XGTI) Technique has been widely used for quantitative phase imaging, X-ray dark-field contrast as well as for X-ray beam characterization.[1-4] One of the main reasons for performing imaging/tomography experiments at synchrotron facilities is to carry out dynamic measurements. The standard two-grating measurement has the disadvantage of lower signal to noise ratio since we need at least three grating steps per projection to encode phase information in the intensity measurement.[5] A single phase-grating phase-stepping technique can be used, however; the stepping technique is not compatible with fast imaging. Therefore, we have been using single phase-grating spatial harmonic imaging technique[6] for performing these experiments. This technique was first invented by M. Takeda et al[7] for the visible light and later H. Wen et al[8] applied to X-ray imaging field where they used a single two-dimensional transmission grid.

We have explored the idea of using pink beam having broader wavelength spectrum for dynamic imaging.[9] This gives us the chance to explore the timescales for a dynamic experiment beyond what was possible before with added advantage of having a very stable beam. Associated with this change is the spatial coherence of the beam. The single grating XGTI is ideal for determining this change in spatial coherence by measuring the visibility of the interference pattern downstream of the grating at different Talbot distances.[3] This decay in the visibility over different Talbot distances provides the estimation of the X-ray beam spatial coherence. A comparison with the monochromatic beam provided by the Multi-Layer monochromator (MLM) will be presented.

XGTI is routinely applied for imaging of soft tissue samples. The dark-field and the quantitative phase information permit easier segmentation of the samples and identifying distinct tissue and other features. New science is addressed by

the most recent instrumental development. We studied the crystallization process in a fluid system, forced by the addition of an anti-solvent liquid. The early stages and different processes involved in crystallization can be observed. We will also show phase tomography images of an orchid bee head. New scientific and technical opportunities presented due to Diamond Light Source upgrade to Diamond II and in light that beamline I13 figures as one of the flagship projects will be elucidated. In particular, we have a sample changer robot that was installed recently which should aid in high-throughput imaging.

2. EXPERIMENTAL SETUP

The main two aspects for high-speed imaging that we describe here are higher flux and faster acquisitions. We have addressed this by using the filtered pink X-ray beam (broad X-ray wavelength spectrum with higher flux) and using spatial harmonic imaging technique.[6]

2.1 X-ray Beam conditioning

For producing a Talbot image from an X-ray grating, we need to use monochromatic beam. However, it has been shown that one can use polychromatic sources[10], though with reduced visibility. The X-ray beam for I13-2 is provided by an U22 undulator source, which is reflected by an X-ray mirror positioned at about 25 m. This has three stripes, Si (Silicon), Rh (Rhodium) & Pt (Platinum). Since we have used 15 keV energy for visibility measurement, as explained in section 4.1, Si stripe was used which has the better reflectivity at this energy and also removes the higher harmonics. For the dynamic radiographic measurement of anti-solvent crystallization we have used the Rhodium mirror so that we can have higher reflectivity at 19 keV X-ray energy. Because of the unique X-ray source spectrum of an undulator, for a given energy we can select an undulator gap which gives the highest flux. We have used 11.09 mm and 6.185 mm undulator gaps respectively for 15 and 19 keV. Beside the carbon filters, which are commonly used to absorb soft X-ray's or any energies lower than this, Al of 1.4 mm and Y of 50 μm are used to cut the undulator harmonic peaks below 15 keV and above 17 keV respectively. Whereas for the 19 keV we had Al 0.7 mm and Mo of 84 μm. Reference 11, figure1 provides more details on the spectrum for 15 keV. This filtered X-ray pink beam offers better flux with very stable beam.

2.2 Spatial Harmonic Imaging

We have used single-phase grating and a high-resolution detector system for resolving the interference pattern at first Talbot distance from an X-ray grating. Since the recorded interference pattern contains the grating image, we need to de-convolve the grating image from the sample image. This can be done by the spatial harmonic imaging technique as explained in references 3 and 6-9. Downside for using single-phase grating single-shot technique is that the final image spatial resolution is about 5 times inferior to what we get with normal phase stepping XGTI measurement techniques. However, the data acquisition and processing time is almost 3-5 times lower since we are using only one image to build one single projection of the sample. This is very attractive for the dynamic experiments.

3. EXPERIMENTAL DETAILS

The visibility measurement was performed at 15 keV with $3\pi/2$ phase shifting grating having 4.8μm period. For 19 keV we used a $\pi/2$ phase shifting grating of 4.8 μm period made of Si etched structures (fabricated at the PSI in the X-ray Optics and Applications group). For the dynamic measurements, the grating was placed at the first Talbot distance. The visibility of the gratings with a 4× magnification objective was ~15%. We used a pco.edge 5.5 camera with 8× total optical magnification, which achieves a single pixel size of 0.81μm ×0.81μm.

4. RESULTS AND DISCUSSION

4.1 X-ray beam coherence measurement

The XGTI has been used for the X-ray beam coherence and wavefront characterization before.[3, 12-14] It is expected that with the filtered X-ray pink beam the interference pattern visibility as well as the X-ray beam coherence get affected. Therefore, we did a test looking at the visibility pattern downstream of the grating at different Talbot distances and estimated the X-ray beam coherence for filtered X-ray pink beam as well as MLM (Mo/B$_4$C). As expected, the MLM has slightly better visibility and transverse coherence compared to the filtered pink beam. However, the measured spatial coherence length for the filtered pink beam is much larger than the period of the grating.
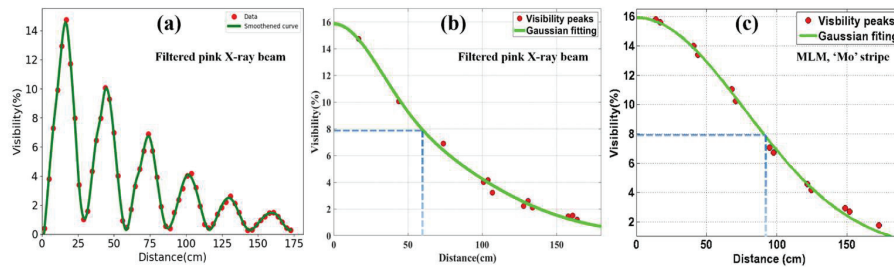
Figure 1. (a) Visibility measurement for pink beam. 1.1(b-c) coherence measurement for filtered X-ray pink beam and MLM Mo/B₄C stripe.

Figure1 shows the comparison of the visibility and coherence measurements for 15 keV pink X-ray beam and the MLM (Mo/B₄C) monochromatic beam. Figure 1(a) shows the visibility map for the filtered pink beam. The grating is placed such that grating lines are parallel to the vertical (y) direction. This implies we are probing the horizontal direction (x) spatial coherence values (i.e., ξ_x). The maximum visibility was achieved at 1st fractional Talbot distance which was 14.6% at 168 mm from the grating. The successive fractional Talbot distances have reduced visibility due to degradation of the X-ray beam spatial coherence. Figure 1(b) shows a Gaussian fit through the peak visibility points of figure 1(a) which provides the decay in the visibility. A similar curve was obtained for the MLM (Mo/B₄C) which is plotted in Figure 1(c). For a $\pi/2$ grating the spatial coherence length can be obtained by ξ_x (exp) = $\lambda\sigma/p$, where, λ = X-ray wavelength, σ = FWHM of Gaussian curve, p= period of the grating. Analytically we can calculate this by the equation ξ_x (ana) = $\lambda D/2\pi p\sigma_x$, where D = distance between source and the grating position and σ_x= divergence of the x-ray beam. Detailed discussion on spatial coherence measurement can be found here[3, 12-14]. Inputting the relevant values in the above equations, the ξ_x (exp) is found to be 10.1 μm and 15.2 μm for the pink and the monochromatic beams, respectively. The analytical calculation gives us the value of 12.6 μm. This agrees well with what is predicted.

4.2 2D dynamic imaging of anti-solvent crystallization
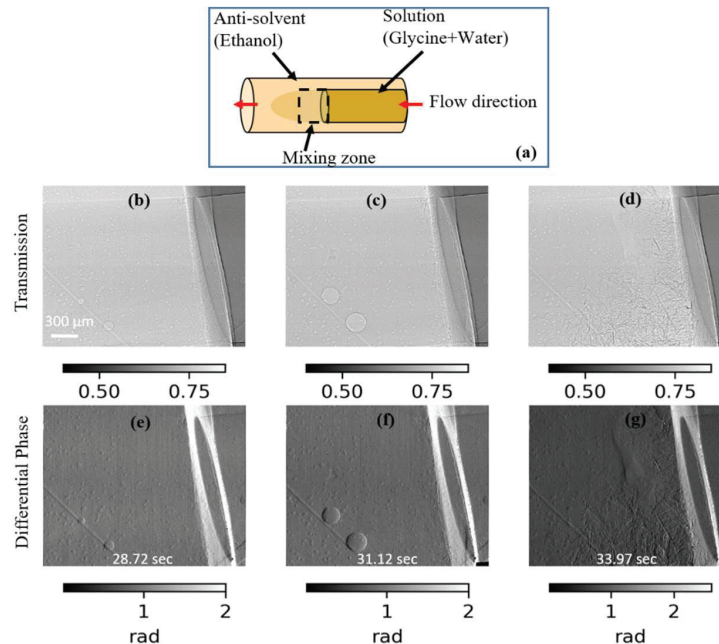

Figure 2. Anti-solvent crystallization of glycine in ethanol. 2(a) Shows a schematic of the experimental setup. 2(b)-(d) transmission images at three different points of a time lapse series. We can see the crystal formation at the edge of tubing and later at the mixing zone. 2(e)-(f) Differential phase contrast images at same intervals forming a thin-layer in the mixing zone.

The filtered X-ray pink beam was used for dynamic imaging of an anti-solvent crystallization process using a continuous flow microreactor. In this reactor a solution of the crystallizing organic compound is fed continuously through an inner concentric tube (3 mm OD) into the flow of a second solvent that reduces the solubility of the product (anti-solvent) and thus causes its crystallization. The outer tube containing the anti-solvent flow was a 6 mm OD Kapton tube. The objective was to use the contrast mechanisms of XGTI to visualize nucleation and growth of crystals in the mixing zone downstream of the inner tube mouth, where the solution is fed into the antisolvent flow, (Fig 2(a)). Experimentally, the inner tube feed was aqueous glycine (232.89 g/kg; equivalent to a supersaturation ratio of 2.76), while an ethanol anti-solvent was in the outer flow tube, with inner/outer flow rates in a 3:1 ratio. The images were taken at exposure time of 50 ms at a rate of 17 Hz. XGTI revealed that instead of mixing and homogeneous nucleation a number of heterogeneous nucleation and crystallization processes takes place in this system. Examples include rapid nucleation at the nozzle surfaces and at the weld edges of the Kapton tube. The reconstructed transmission (Fig. 2(b-d)) and the differential phase (Fig. 2(e-g)) shows how the nucleation first happens at the nozzle and later begins at the mixing zone. Besides the crystal formation, a thin layer is formed in the mixing zone which we can clearly see in the differential phase image, especially Figure 2(f), and this is not clear in the transmission image. The walls of the Kapton tube have shown traces of deposits, which tends to hinder the visualization of differential phase as well the transmission images slightly. We are looking at different solutions for the tubing and avoiding the nucleation at edges.

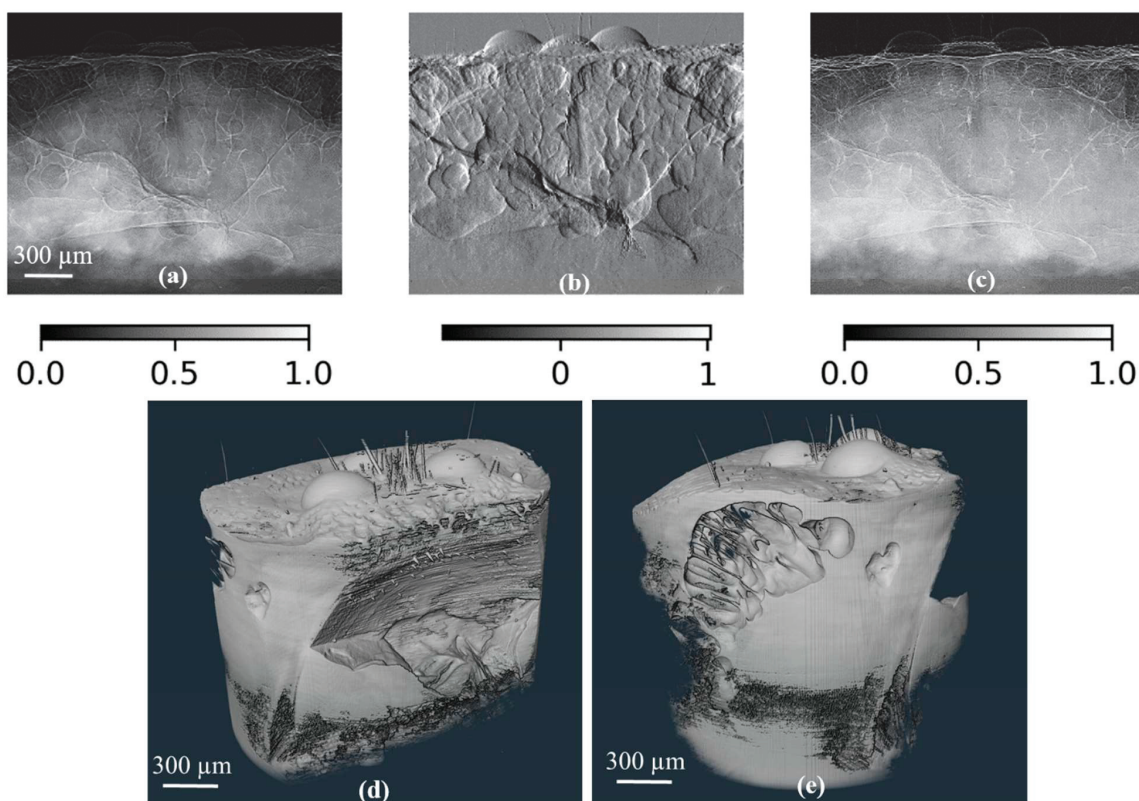### 4.3 3D Tomography of Orchid-bee head

Figure 3. Reconstructed images of an orchid bee head using pink beam single grating X-ray Talbot interferometer. (a) absorption (b) differential phase (rad) and (c) dark-field images of the first projection image. Differential phase image has rich signal as shown in image (b). Also noticeable in (c) is dark-field signal at edges and boundaries. 2(d)-(e) Three-dimensional rendering of the reconstructed phase image. The three ocelli on the top with part of the compound lens surrounding it is clearly visible.

Orchid bees could fly in cluttered environments, for example in rain forest under low light conditions. However, it is unclear as to what visual information they use for flight control. A recent absorption micro-tomography study performed on the orchid bee ocelli at our beamline inferred that ocelli perform dual functions, detecting focused light and unfocussed polarized light to guide them through these challenging conditions.[15] We have already shown that the technique mentioned above is very useful for high-speed 2D imaging.[9] Extending this we demonstrate that performing rapid tomography acquisitions is also possible. An Orchid bee head sample was used to perform phase tomography using the filtered pink beam single grating X-ray Talbot interferometer.

Figure 3 shows reconstructed images of the top of an orchid bee head using filtered pink beam and single grating X-ray Talbot interferometer. Images were acquired at 19 keV with ID gap of 9.5 to get the best imaging condition. Detector was placed at the first Talbot distance and images were collected with 1 sec exposure over 0 to 180° interval with 3000 projection angles. From each projection image, we reconstructed the transmission, differential phase and dark-field signal images, as detailed in reference 3 and 7. Reconstructed differential phase images were converted to phase volume by first integrating using the Hilbert filter and later applying filtered back-projection (FBP) algorithm. All these reconstruction processes are performed using savu, a tomography reconstruction and processing pipeline.[16] Figure 3(a) shows the absorption image, 3(b) the differential phase (rad) and 3(c) dark-field images of the first projection image. Differential phase image has rich signal as shown in image indicating that the new method for grating interferometer data measurement is suitable for phase samples. Three-dimensional rendering of the reconstructed phase image is shown in figure 3(d)-(e). The three ocelli on the top with part of the compound lens surrounding it is clearly visible.

The Orchid bee head sample used here was stained; however, it would be interesting to look at the unstained samples. Further, we would like to look at the nerve bundles descending from retina to better understand how the visual information is processed.

4.4 Sample changer robot

Recently, we have added a sample-changing robot, which can change the sample after each scan without any manual intervention in between. The system consists of a robotic arm that picks the sample from a tray containing 112 samples. Once sample is moved to the tomography stage, the automatic alignment script is run and a predefined tomography scan will be executed. The maximum sample diameter that is possible with the sample transport gripper is 5 mm with maximum
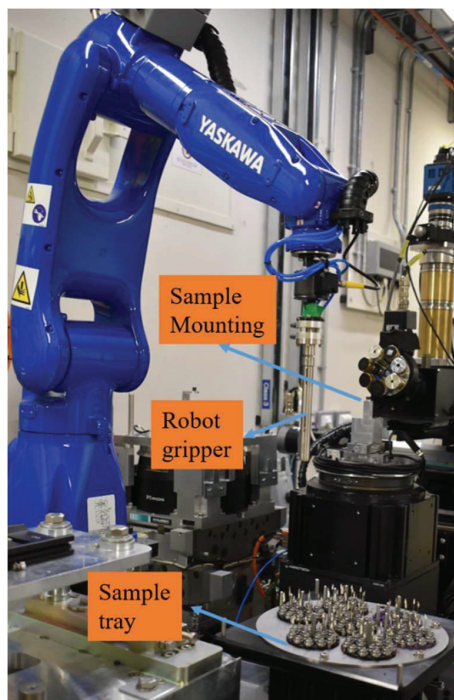

Figure 4. Picture of the sample changer robot installed in the I13-2 Diamond-Manchester Imaging Branchline.

height of 25 mm. Samples are mounted on a barcode engraved sample holder and when the sample is transported from tray to the tomography stage, a laser reads the barcode and identifies the sample to be scanned. Figure 4 shows the picture of the sample changer robot installed in our beamline. For more details, please look at the paper number 11840-49.

Conducting experiments such that statistically relevant data is collected is important in many fields. Therefore, maximum utilization of the available experiment time is important. Use of robot will help with this. In the future using sample-changer robot will aid in running in-situ experiments with sample environments where the sample environment needs to be changed rapidly.

OUTLOOK

The filtered pink X-ray beam has good flux and has enough spatial coherence for doing 2D dynamic grating interferometer. We are in the process of testing filtered pink X-ray beam at different energies with different orientation of the grating lines providing us information on the spatial coherence of the beam in different direction. Tomography reconstruction of the Orchid bee head sample shows that we can obtain phase volume reconstructions using filtered pink beam and this is promising when we want to look at the unstained samples. To improve the flux further installing compound refractive lens (CRL) is also planned. A robot installed for automatically changing the samples at the end of each tomography scan is an important addition for doing high-speed, high-throughput imaging.

ACKNOWLEDGMENTS

REFERENCES

[1] Zdora, M-C., Vila-Comamala, J., Schulz, G., Khimchenko, A., Hipp, A., Cook, A. C., Dilg, D., David, C., Grünzweig, C., Rau, C., Thibault, P., Zanette, I., "X-ray phase microtomography with a single grating for high-throughput investigations of biological Tissue," Biomed. Opt. Express, 8, 1257-1270 (2017).

[2] Bikis, C., Rodgers, G., Deyhle, H., Thalmann, P., Hipp, A., Beckmann, F., Weitkamp, T., Theocharis, S., Rau, C., Schulz, G. and Müller, B., "Sensitivity comparison of absorption and grating-based phase tomography of paraffin-embedded human brain tissue," Applied Physics Letters 114(8), p.083702 (2019)

[3] Marathe, S., Shi, X., Wojcik, M.J., Kujala, N.G., Divan, R., Mancini, D.C., Macrander, A.T. and Assoufid, L., "Probing transverse coherence of x-ray beam with 2-D phase grating interferometer," Optics express 22(12), p14041-14053 (2014)

[4] Rutishauser, S., Samoylova, L., Krzywinski, J., Bunk, O., Grünert, J., Sinn, H., Cammarata, M., Fritz, D.M. and David, C., "Exploring the wavefront of hard X-ray free-electron laser radiation," Nature communications 3(1), p.1-6 (2012)

[5] Weitkamp, T., Diaz, A., David, C., Pfeiffer, F., Stampanoni, M., Cloetens, P. and Ziegler, E., "X-ray phase imaging with a grating interferometer," Optics express 13(16), p.6296-6304 (2005).

[6] Marathe,S., Zdora, M-C., Zanette, I., Cipiccia, S., Rau, C., "Comparison of data processing techniques for single-grating x-ray Talbot interferometer data," Proc. SPIE, 103910S (2017)

[7] Takeda, M., Ina, H. and Kobayashi S., "Fourier-transform method of fringe-pattern analysis for computer-based topography and interferometry," J. Opt. Soc. Am. **72**, 156-160 (1982)

[8] Wen, H. H., Bennett, E. E., Kopace, R., Stein, A. F., Pai, V., "Single-shot x-ray differential phase-contrastand diffraction imaging using two-dimensional transmission gratings," Opt. Lett., **35**, 1932-1934 (2010)

[9] Marathe, S., Storm, M., Kuppilli, V. S. C., Harrison, R., Das, G., Schroeder, S. L. M., Cipiccia, S., Döring, F., David, C., Rau, C., "Development of synchrotron pink beam x-ray grating interferometer at the Diamond Light source I13-2 beamline," Proc. SPIE 1111319 (2019)

[10] Momose, A., Yashiro, W., Harasse, S. and Kuwabara, H., "Four-dimensional X-ray phase tomography with Talbot interferometry and white synchrotron radiation: dynamic observation of a living worm," Optics express 19(9), p8423-8432 (2011).

[11] C. Rau, M. Storm, S. Marathe, A. J. Bodey, M. Zdora, S. Cipiccia, D. Batey, X. Shi, S. M. L. Schroeder, G. Das, M. Loveridge, R. Ziesche, B. Connolly, "Fast Multi-scale imaging using the Beamline I13L at the Diamond Light Source," Proc. SPIE 111130P (2019)

[12] Guigay, J.P., Zabler, S., Cloetens, P., David, C., Mokso, R. and Schlenker, M., "The partial Talbot effect and its use in measuring the coherence of synchrotron X-rays," Journal of synchrotron radiation *11*(6), p.476-482 (2004)

[13] Pfeiffer, F., Bunk, O., Schulze-Briese, C., Diaz, A., Weitkamp, T., David, C., Van der Veen, J. F., Vartanyants, I. and Robinson, I. K., "Shearing Interferometer for Quantifying the Coherence of Hard X-Ray Beams," Physical Review Letters 94, 164801(2005)

[14] Diaz, A., Mocuta, C., Stangl, J., Keplinger, M., Weitkamp, T., Pfeiffer, F., David, C., Metzger, T.H. and Bauer, G., "Coherence and wavefront characterization of Si-111 monochromators using double-grating interferometry," Journal of synchrotron radiation 17(3), p299-307 (2010)

[15] Taylor, G. J., Ribi, W., Bech, M., Bodey, A. J., Rau, C., Steuwer, A., Warrant, E. J., Baird, E., "The Dual Function of Orchid Bee Ocelli as Revealed by X-Ray Microtomography," Current Biology 26(10), p1319-1324 (2016)

[16] Wadeson, N. and Basham, M., "Savu: a Python-based, MPI framework for simultaneous processing of multiple, N-dimensional, large tomography datasets," https://arxiv.org/abs/1610.08015 (2016)